MODELING THE LOW-ALTITUDE TRAPPED RADIATION ENVIRONMENT

Shing F. Fung[1], Daniel M. Boscher[1,2], Lun C. Tan[1,3] John F. Cooper[1,3]

and

David S. Evans[4]

[1]Space Physics Data Facility, NASA Goddard Space Flight Center, Greenbelt, MD 20771, USA
(shing.fung@gsfc.nasa.gov; Fax: 301-286-1771)
[2]CERT-ONERA, Toulouse, France
[3]Also at the Hughes STX Corporation, Greenbelt, Maryland, USA
[4]Space Environment Center, Boulder, Colorado, USA

ABSTRACT

Knowledge of the trapped energetic particle radiation at low altitudes (<1000 km), particularly in the vicinity of the South Atlantic Magnetic Anomaly region, is important for studying the space environmental effects on space systems in this region. Standard empirical models, such as the NASA AP-8 model for protons and the AE-8 model for electrons constructed more than two decades ago, are dated and are deficient in this region because of the lack of long-term data coverage and the presence of steep atmospheric and magnetic cutoffs at low altitudes. Recent analyses of the trapped particle data at energies up to a few MeV taken from the Japanese OHZORA (1984-87) and NOAA-10 (1986-91) satellites (both at altitudes up to 850 km) have revealed that the long-term trends in the observations are generally consistent with the NASA trapped radiation models, though individual measurements may differ significantly from the models. The discrepancies between the observations and the standard trapped radiation models are being investigated by using a three-dimensional diffusive model and realistic atmospheric and magnetic field models. In this paper, we will show the results of inter-comparisons among the observations, diffusive model calculations and the NASA models. We will also outline the requirements for future efforts in modeling the low-altitude trapped radiation environment.

1. INTRODUCTION

Energetic electrons and ions (> tens of keV) trapped in the terrestrial magnetic field, forming the Van Allen Radiation Belts, are hazardous to both manned and unmanned space missions [Spjeldvik and Rothwell, 1985; McCormack, 1988; Baker *et al*, 1994]. While lower energy (< 1 MeV) particles can cause surface charging on spacecraft and the instruments aboard, leading to arching discharges and affecting instrument performance, higher energy (1–10^2 MeV) particles can penetrate the spacecraft, damaging the various subsystems, including onboard computer chips and biological tissues. In addition, the trapped radiation also leads to high background levels in x-ray and gamma-ray astrophysical measurements. Therefore, having a good understanding of and the capability to "predict" the radiation environment likely to be encountered by a space vehicle are crucial for the design, planning and operations of space missions as well as the analysis of space science data.

The existing NASA trapped radiation models [Vette, 1991a], the AP-8 model for protons [Sawyer and Vette, 1976] and AE-8 model for electrons [Vette, 1991b] developed in the 1970's and 1980's, have been widely distributed and used for various space mission planning and spacecraft engineering applications. Due to limited capabilities in early data management technology (storage, manipulation, and dissemination) and in the analysis tools at the time when the models were developed, gross averaging of the data was necessary to reduce the data volume to manageable sizes. As a result, the existing models are static and highly averaged, with little adaptability to applications with varying geomagnetic conditions. Thus, there are significant discrepancies, particularly at low altitudes and low L-shells (L<3), between the models and observations of the space radiation environment [see *e.g.*, Fung, 1996; Fung *et al.*, 1996; Boscher *et al.*, 1996]. With more sensitive and miniaturized instruments and electronics being flown on more complex missions,

ESA Symposium Proceedings on 'Environment Modelling for Space-based Applications', *ESTEC, Noordwijk, NL, 18-20 September 1996* (SP-392, December 1996)

their increasing susceptibility to space radiation effects calls for an urgent need to develop the next generation of trapped radiation models for assessing the space radiation environment.

The development of a new generation of magnetospheric state-based trapped radiation models has been proposed recently by Fung [1996]. Providing that sufficient data are available, two outstanding technical issues confront the construction of large-scale empirical trapped radiation models. First, many different data sets obtained by various instrumentations, having different data formats and hosted in different storage platforms, must be combined and statistically analyzed in order to construct the models. It is therefore critical to process all the data to some degree of conformity such that they are inter-comparable before meaningful statistical analysis can be performed. This also includes choosing an appropriate coordinate system to display and analyze the data and sorting the data according to their associated geomagnetic conditions. Second, because of the large volume and complexity (multi-dimensionality) of the particle and associated ancillary data, data management facility and analysis tools must meet the data storage requirements and support rapid data accessibility and manipulations. As described in Fung [1996], these technical issues can in principle be overcome by using state-of-the-art data management tools based on the Common Data Format (CDF) [Kessel et al., 1994a,b].

As discussed in Fung [1996], one factor inherent to the deficiencies in the existing NASA trapped radiation models is the lack of long-term monitoring data sets with sufficient spectral and spatial coverage. This remains to be the case particularly in the low altitude (<1000 km) region despite the availability of more recent data since the times when the existing models were constructed. Although new empirical models are being developed based on the recent CRRES data [*e.g.*, Gussenhoven *et al.*, 1996], we are still a long way from having a completely operational set of models that can account for most, if not all, of the observed trapped radiation phenomenology, such as in its temporal, spatial and spectral variations [Li *et al.*, 1993; Baker *et al.*, 1994; Fung *et al.*, 1996].

In order to model the radiation environment, numerical models have been constructed to simulate the physics of trapped radiation transport and loss processes [*e.g.*, Beutier and Boscher, 1995; Beutier *et al*, 1995]. Since Coulomb interactions are relatively straightforward when the corresponding interaction cross sections are provided, more uncertainties are involved with the wave-particle interaction and diffusive processes. This paper examine the effects of radial, pitch-angle, and energy diffusion on the spatial distribution of trapped electrons at low altitudes.

In the following sections, we will first compare the current NASA trapped radiation models, AP-8 and AE-8, with recent energetic particle measurements from the NOAA-10 and the Japanese OHZORA satellites, and then describe some recent results from physical modeling with the Salammbo model [Beutier and Boscher, 1995].

2. COMPARISON BETWEEN NASA TRAPPED RADIATION MODELS AND LOW ALTITUDE MEASUREMENTS

The NASA empirical trapped radiation models have been in existence for over two decades. Details of the models are described in Sawyer and Vette [1976], Vette [1991a,b] and, more recently, Fung [1996]. To compare the models with observations, we have processed the energetic proton data (0.03-2.5 MeV) from NOAA-10 and the energetic electron data (0.19-3.2 MeV) from OHZORA. In order to extract the measurements of the trapped population, we have analyzed the data by assuming a canonical pitch angle distribution of the form $J(\alpha) = J_{\perp}\sin^{N}(\alpha)$ for the directional fluxes of the trapped particles, where α is the local pitch angle of the particles, $J_{\perp}$ is the particle flux at $\alpha = 90°$, and N is the anisotropy index. We have also improved upon the conventional analysis techniques [Fischer *et al.* 1977; Nagata *et al.*, 1985; Kohno *et al.*, 1990] by incorporating the pitch angle anisotropy of the measured particles into the calculation of the detector geometric factors such that more representative particle fluxes are obtained at different pitch angles [Tan *et al.*, 1996].

Figure 1 shows a comparison between the energetic trapped proton measurements (E > 250 keV) obtained in October-December 1986 by the NOAA-10 satellite and the AP-8 MIN model based on the 1986 IGRF magnetic field model. The orientation of the NOAA-10 orbit was such that proper measurements of the trapped population by the two nearly-orthogonal telescopes of the Medium Energy Proton and Electron Detector (MEPED) [Seale and Bushnell, 1987] could only be made in the L-shell range of L < 4.5 [Tan *et al.*, 1996]. Nevertheless, the model is consistent with the omnidirectional fluxes (grey data points) seen by NOAA-10 in 2 > L > 4, where the anisotropy index N remains relatively constant (N ≈ 10). At lower L values (L < 2), the dramatic decrease in N indicates possible contamination by more energetic (> 10 MeV) protons in the

measurements (dark data points with N < 6).

As N remains relatively constant for L > 2 as indicated in Figure 1, it is possible to calculate the omnidirectional fluxes at L > 4 by using the form of the pitch angle anisotropy assumed above and the observations from one of the MEPED telescopes. The results are summarized in Figure 2 for 0.03-2.5 MeV with the data points below about L = 2 removed.

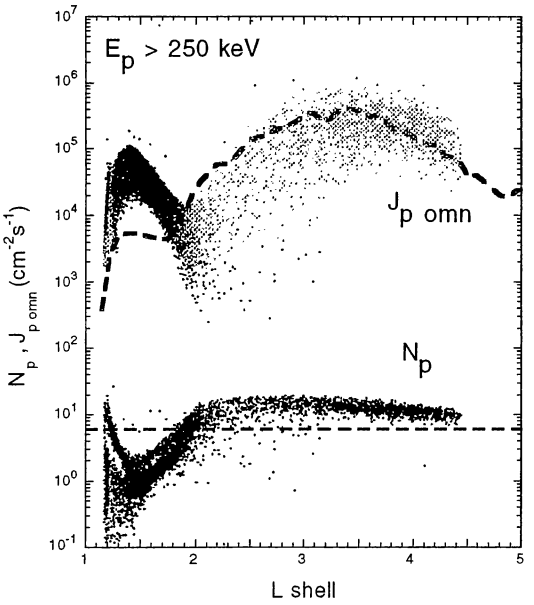

Figure 1. L-shell profiles of omnidirectional fluxes and anisotropy indices of > 250 keV trapped protons observed by the NOAA-10 satellite. The dark data points a L< 2 with N < 6 indicate the contamination by the more energetic (> 10 MeV) protons.

The NOAA-10 observations at the various energies shown in Figure 2 are remarkably consistent with the respective L-shell profiles given by the AP-8 MIN model, despite the uncertainties in mapping the model fluxes to the NOAA-10 altitude (nominally 833 km) [Raben *et al.*, 1995] and in extrapolating N to higher L-shells. Since the AP-8 model has a lower energy limit of 0.1 MeV, no comparison to the model can be done at 0.03 MeV. It is interesting to note, however, that the AP-8 MIN model for both the 1986 (left panel in Figure 2) and the original 1964 (right panel) epochs are within the respective ranges of the data, indicating that the low-altitude trapped proton environment is relatively insensitive to long-term secular changes. This is contrary to the apparent increase in the trapped proton fluxes seen in a comparison of the 1989 NOAA-10 observations and the AP-8 MAX (1970, 1989) models [Fung, 1996].

Next, we compare the trapped electron observations (0.19-3.2 MeV) obtained in 1984-1987 by the low-altitude OHZORA (350-850 km) and NOAA-10 (833 km) satellites in 1986 to the NASA AE-8 MIN model. The analysis technique and the global distributions of low-altitude trapped electrons observed by OHZORA have been described recently by Fung *et al.* [1996] and Tan *et al.* [1996]. Furthermore, Fung *et al.* [1996] have also indicated the presence of local-time variations in both the trapped electron fluxes and pitch angle distributions, particularly near the quiet-time slot region (L=2-3; see e.g., Lyons and Thorne, [1973]). In this paper, we will focus on the low altitude L-shell distributions of trapped electrons

Figure 3 shows an inter-comparison between the OHZORA and NOAA-10 observations of omnidirectional electron fluxes and anisotropy indices as a function of L at E > 0.1 MeV. It should be noted that the NOAA-10 electron detectors were sensitive to 0.135-1 MeV incident proton fluxes, which have been corrected in our analysis by subtracting the corresponding measurements from the directional proton detectors, as suggested by Raben *et al.* [1995]. It is apparent that the OHZORA and NOAA-10 observations are quite consistent both in the flux levels and in the anisotropy indices N (right panels). The AE-8 model fluxes are superposed as dark-dashed lines in the left hand panels of Figure 3 for comparison. It seems that the model, when being applied to the low altitude region, tends to over-predict slightly the flux levels in the higher L-shells (L > 5), while remaining within bounds of the data. The model slot region is also shifted inward by about ΔL=0.5 as compared to the observations.

3. LOW-ALTITUDE ATMOSPHERIC OR MAGNETIC CUTOFF

Trajectories of trapped particles at low altitudes (< 1000 km) are affected mostly by the residual atmosphere and the sharp magnetic gradients near their mirror points. Within the bottomside ionosphere (<400 km), collision processes are the dominant mechanism responsible for the loss of trapped electrons. For most practical purposes, trapped electrons which reach the altitude of 100 km are considered to be effectively lost into the atmosphere. Thus this limiting or cutoff altitude provides an effective lower boundary to the trapped electrons fluxes.

Based on a given magnetic field model, the lower trapping boundary (at a constant cutoff altitude) can

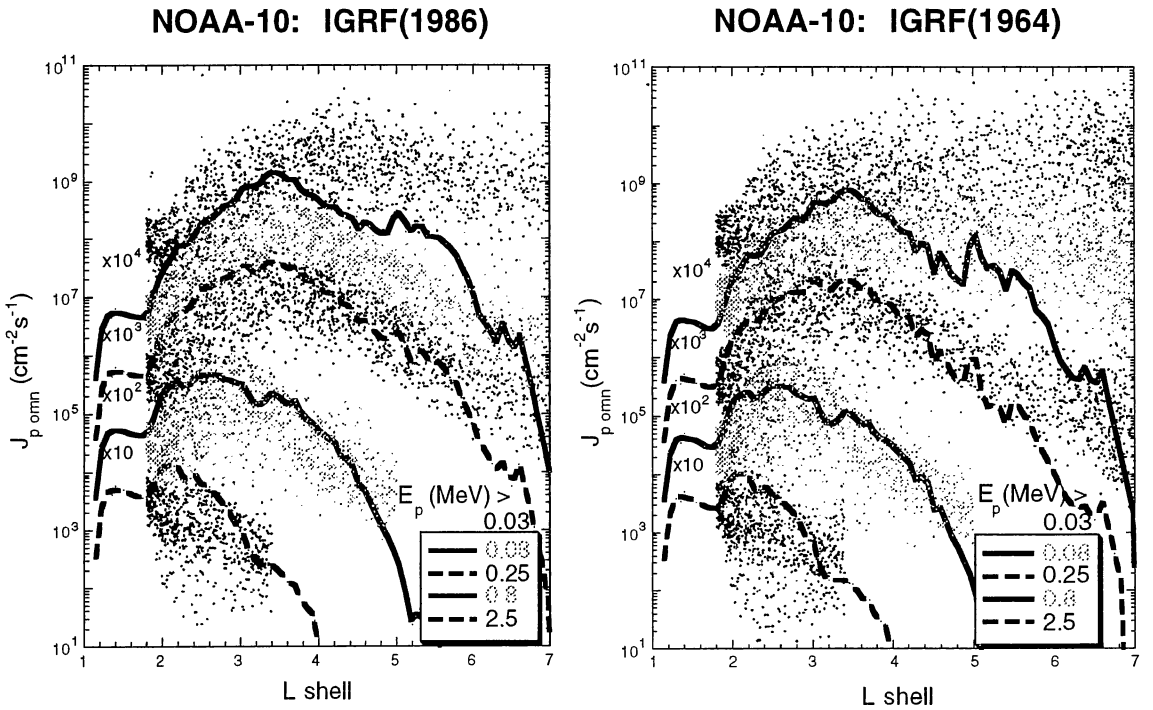

Figure 2. Comparisons between NOAA-10 trapped proton observations and the NASA AP-8MIN model at $E_p > 0.08$, 0.25, 0.8 and 2.5 MeV. No significant difference is seen in the two AP-8MIN models based on the IGRF(1986) (left) and the IGRF(1964) (right).

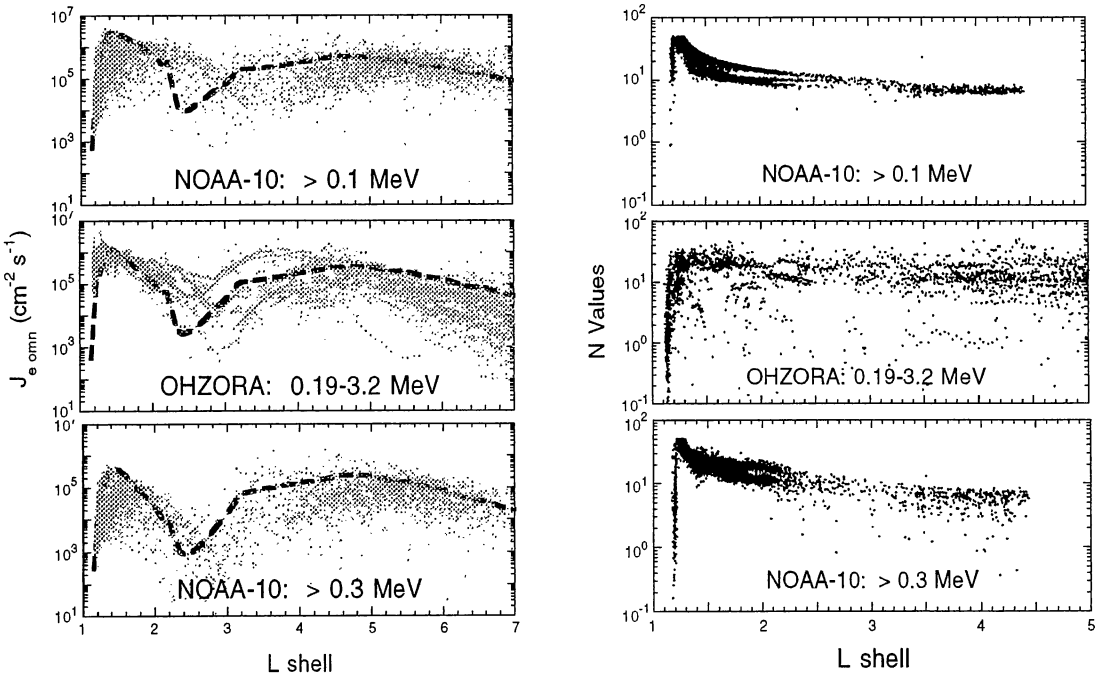

Figure 3. Inter-comparisons between the trapped electron observations from the NOAA-10 and OHZORA satellites.

be expressed in terms of a simple magnetic cutoff function of the magnetic coordinates. For a dipolar magnetic field, for example, the magnetic cutoff is given by $B_c/B_0 = L^3[4 - (3/L)]^{1/2}$, where B_c is the field strength at the cutoff altitude, B_0 is the field strength at the magnetic equator, and L is the McIlwain parameter. The magnetic cutoff function implemented in the NASA AE-8 model has largely been determined empirically from the AZUR satellite data (387-3150 km; Nov. 1969–Mar. 1970) and is given by [Vette, 1991b]:

$$\frac{B_c}{B_0} = b_{c2}(L) = \begin{cases} 0.6572\ L^{3.452}\ ; & 1.2 \le L < 2.4 \\ 0.196\ \ L^{4.878}\ ; & 2.4 \le L \le 3.0 \\ 1.4567\ L^{3.050}\ ; & L > 3.0 \end{cases} \quad (1)$$

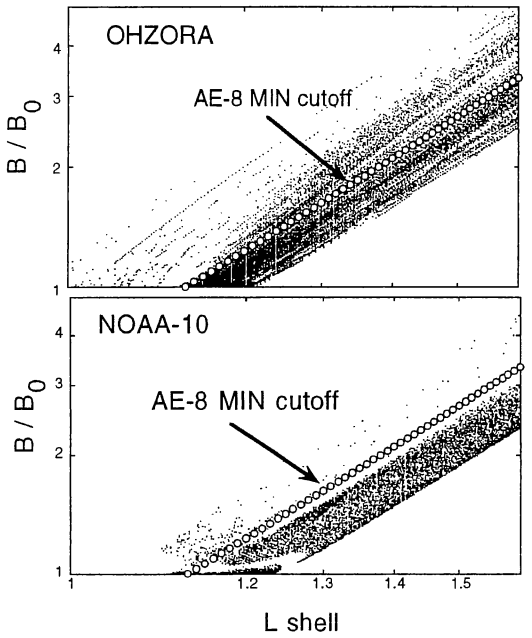

Figure 4. Magnetic coordinates (B/B_0 , L) of OHZORA (upper panel) and NOAA-10 (lower panel) based on the IGRF(1986) magnetic field model, at which significant trapped electron fluxes (much higher than background level and with N≈10) were observed. Open circles mark the AE-8 magnetic cutoff given in Equation (1).

Using the IGRF(1986) model, we have obtained and plotted in Figure 4 the magnetic coordinates (B/B_0, L) of the OHZORA (upper panel) and NOAA-10 (lower panel) satellites below L=1.6 at which significant trapped electron fluxes (with N >> 1) were observed.. The superposed open circles indicate the corresponding AE-8 magnetic cutoff for L ≤ 1.6 (see Equation 1). While most of the NOAA-10 observations remained above the AE-8 cutoff (*i.e.*, with lower B/B_0 and/or higher L), numerous OHZORA data points with significant trapped electron fluxes are seen below the AE-8 cutoff. The OHZORA and NOAA-10 observations shown in Figure 3 have been chosen from observation points with local $B/B_0 = 0.85\ b_{c2}$ (Equation 1).

To investigate the performance of the AE-8 model near the magnetic (atmospheric) cutoff, we have plotted the L-shell profiles of the omnidirectional fluxes of trapped electrons (0.19-3.2 MeV) observed by OHZORA above, at, and below the AE-8 cutoff (dashed curves) and the results are shown in Figure 5. It is clear that significant deviations of the AE-8 model from the observations occur at L < 2.5 in all three cases, particularly below the cutoff (lower panel) where the model flux levels are at least four orders of magnitude short of the observed levels.

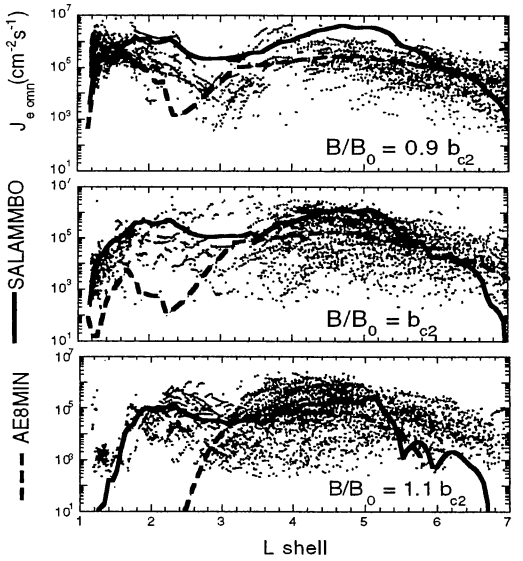

Figure 5. L-shell profiles of trapped electrons (0.19-3.2 MeV) observed by OHZORA at 350-850 km during quiet times ($|D_{st}|$<30nT) in 1984-87. The corresponding profiles along three different low altitude trajectories (magnetic cutoffs) as computed from the Salammbo and NASA AE-8MIN models are shown in solid and dashed lines, respectively.

4. MODELING THE TRAPPED ELECTRON ENVIRONMENT: THE SALAMMBO CODE

In this section, we describe some early results obtained recently on modeling the low-altitude trapped electron environment by using the Salammbo model [Beutier and Boscher, 1995; Boscher *et al.*,

1996]. Salammbo is a three-dimensional model based on the classical Fokker-Planck diffusion equation used to calculate the electron transport in the region of magnetosphere with $1.02 < L < 7$, where L is the generalized McIlwain parameter [Beutier and Boscher, 1995]. The full three-dimensional model in phase space is necessary to properly treat pitch angle diffusion of electrons, either given by Coulomb collisions or by wave-particle interactions. In the model, the transport equation in the three phase space coordinates (the relativistic magnetic moment M, the second invariant J and the shell magnetic flux; see *e.g.,* Roederer [1970] and Schulz and Lanzerotti, [1974]) is solved numerically. The explicit finite differencing scheme with logarithmic steps in M, J, and L for solving the transport equation has been described in detail in Beutier and Boscher [1995]. The Salammbo model fully treats radial and pitch angle diffusion as well as frictional interactions with free (plasmaspheric) and bounded (exospheric) electrons.

The friction terms and pitch angle transport coefficients have been calculated using an eccentric tilted dipole field consistent with the International Geomagnetic Reference Field (IGRF) for 1986 to provide the correct epoch for comparing with the OHZORA observations. The lower atmospheric boundary model is given by an exospheric model derived from the Mass Spectrometer and Incoherent Scatter (MSIS)-86 model (available from the NASA National Space Science Data Center) which is also used for the Coulomb collision calculations. The upper boundary of our model is located at L = 7 with the equilibrium trapped electron fluxes prescribed by the NASA AE-8MIN model [Vette, 1991b]. The radial diffusion coefficients (appropriate for the magnetic and electric perturbations) used were a factor of 10 less than those given in Schulz [1991] in order to obtain good flux agreement in the inner belt region; *i.e.*, $D_{LLM} = 8.0\ 10^{-15}\ f(y)\ L^{10}$ and $D_{LLE} = 1.2\ 10^{-16}$ $g(y)\ h(M,y,L)\ L^{6}$, where the functions f(y), g(y) and h(M,y,L) are as given in Schulz [1991].

The pitch angle diffusion coefficients were calculated as in Lyons *et al.* [1972], but with wave characteristics as deduced from Thorne *et al.* [1973], *i.e.,* an average wave amplitude of 35 nT, a mean frequency of 190 Hz, a bandwidth of 400 Hz and a lower cutoff frequency of 140 Hz. In order to obtain a dayside slot region consistent with observations [Fung *et al.,* 1996], the wave distribution in L-shell was taken to have a trapezoidal form shown in Figure 6 where the maximum value corresponds to the observed average amplitude.

The electron distribution functions were initially assumed to be zero everywhere in the computation box (L between 1.02 and 7). Then the code runs until a steady state is obtained. The resultant distribution functions are then converted into uni- or omnidirectional fluxes. For comparisons with observations and the AE-8 model, integral omnidirectional fluxes (in $cm^{-2}s^{-1}$) were calculated.

Because of the presence of steep loss gradients in the low altitude region, it was necessary to increase the spatial resolution of the original Salammbo model [Beutier and Boscher, 1995]. Table 1 summarizes a comparison of the old and new resolutions, and estimated maximal errors of the Salammbo model in different L ranges, both at the OHZORA altitudes and at the equator.

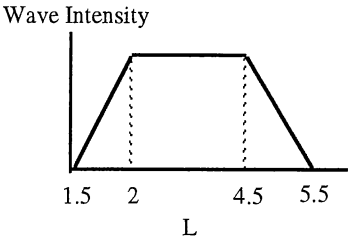

Figure 6. Model L-shell distribution for plasmaspheric hiss

Table 1(a) and 1(b) Improvement of the spatial resolution in the model to compare to OHZORA measurements and estimate of the maximum error due to the resolution:

(a) at the mean OHZORA altitude

L	old			new		
	vertical (km)	horiz. (km)	error (%)	vertical (km)	horiz. (km)	error (%)
1.2	150	630	700	20	290	100
3.5	2400	1800	600	260	920	70
7	3500	3500	1500	300	1700	150

(b) at the magnetic equator

L	old			new		
	vertical (km)	horiz. (km)	error (%)	vertical (km)	horiz. (km)	error (%)
1.2	630	20	700	290	20	100
3.5	1800	60	20	920	60	10
7	3500	120	60	1700	120	30

5. MODEL RESULTS

The global distributions of trapped electrons obtained from the Salammbo model have been calculated recently by Boscher *et al.* [1996], which can be compared directly to the OHZORA satellite observations (0.19-3.2 MeV) [Fung *et al.*, 1996; Tan *et al.*, 1996]. Comparisons of these and additional results to flux levels from the NASA AE-8MIN model and the OHZORA observations are summarized below in Figures 5, 7, 8 and 9.

While Figure 5 shows significant departure of the AE-8MIN model from observations at low L and low altitudes, it also shows that the Salammbo model calculations provide rather reasonable comparisons to the OHZORA measurements, particularly in the vicinity of the AE-8 magnetic cutoff, $b_{c2} = 0.6572\ L^{3.452}$ for $1.2 < L < 2.4$, which was taken as a virtual trajectory in the L-B/B_0 plane (where B is the local magnetic field strength).

For very low altitude trajectories (bottom panel of Figure 5), quite different relative performances of the models are seen in the low L-shell range (L < 3). The AE-8 model predicts vanishingly small population of trapped electrons, but both the Salammbo model and observations are at least two orders of magnitude higher in fluxes. Above the AE-8 cutoff (top panel), the AE-8 model is consistent with the OHZORA observations except for a displacement of the slot region ($\Delta L \sim 0.5$); but the Salammbo model predicts the trapped electron fluxes to be near the observed upper limits. Near the upper L-shell boundary the Salammbo model seems to perform most poorly below the cutoff between L = 5 and 7. This could be due to deficiencies in AE-8, which was used to set the boundary conditions of the Salammbo code at L = 7, and to the uncertainties in the plasmaspheric hiss distribution (Figure 6).

Figure 5 clearly indicates that the AE-8MIN model is deficient at low L shells (L < 3) and at low altitudes. At L = 2 below the cutoff, a minimum of four orders of magnitude difference in fluxes is found between the measurements and the AE-8MIN model. The Salammbo model is clearly much better, including the prediction of the slot location.

In the outer radiation belt region (3 < L < 5), the low-altitude L-shell profiles computed from both the Salammbo and AE-8 models are quite similar to their equatorial counterparts (see Figure 7 below). Despite their relative discrepancies, both models are consistent with the OHZORA observations. The slightly higher model fluxes than the measurements may be attributed to inaccurate radial diffusion coefficients at low pitch angles or latitudinal wave distributions (Figure 6) in that region. The overall agreement between the Salammbo model and the OHZORA measurements for this altitude (350 - 850 km) and energy range (E > 0.2 MeV) is quite remarkable.

Figure 7 shows a comparison of the equatorial L-shell profiles of integral omnidirectional fluxes of trapped electrons obtained from the Salammbo and the NASA AE-8MIN models. Since the AE-8MIN fluxes were used as boundary conditions at L = 7, the fluxes there from the two models are identical. At lower L values, there is good qualitative agreement between the two models and the discrepancies never exceed a factor of 5. It should be noted that the AE-8 model corresponds only to an average of fluxes which are drastically varying in the outer belt (L > 3) [Baker *et al.*, 1994], and which in turn influence the dynamic structure of the radiation belts at lower L values.

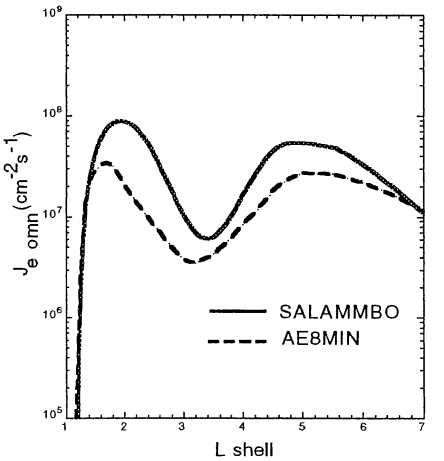

Figure 7. Comparison of equatorial L-shell profiles of omnidirectional trapped electron fluxes (> 0.2 MeV) predicted by the SALAMMBO and AE-8MIN models.

Figure 8 presents model calculations of the global distributions of trapped electron at the altitudes of 400 km (left panel) and 800 km (right panel). The IGRF-86 model has been used to project the results obtained with the tilted dipole field to various locations at a given altitude. We can note here that the distributions shown are qualitatively similar to the distributions measured by OHZORA at the same altitudes shown in Figure 9, particularly in the South Atlantic Anomaly (SAA) region [Fung *et al.*, 1996]. Quantitative discrepancies are seen, however, in both the outer and inner belt regions. At L > 5, the model fluxes are almost a factor of 10 higher than the observations within the longitudinal range of the

SAA. Even lower model fluxes were obtained in other longitudes. These discrepancies may be artifacts of the use of a tilted, but symmetric dipole magnetic field in the model calculations.

At L < 2, the SAA is observed to have a greater latitudinal, but lesser longitudinal, extent than the model results. In this case, we note that the apparent latitudinal extension of the inner radiation belt may have resulted from contamination of the OHZORA electron measurements by high energy protons. The horn in the distribution at 800 km in the northern part of South America appears also in the observations [Fung *et al.*, 1996].

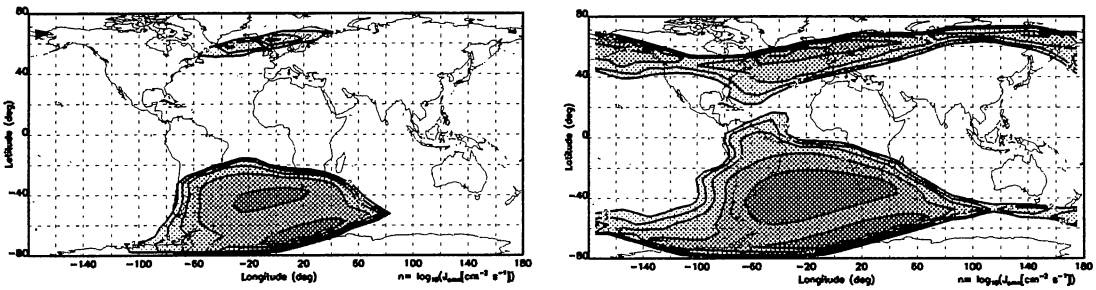

Figure 8. Model calculations of global distributions of omnidirectional fluxes of trapped electrons (> 0.2 MeV) at 400 km (left) and 800 km (right). The five contour levels vary logarithmically from 10^2 to 10^6 $cm^{-2}s^{-1}$ (from Boscher *et al.*, 1996).

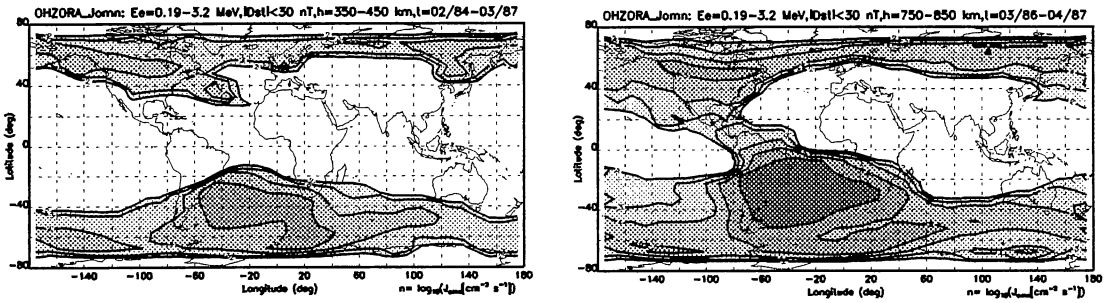

Figure 9. Global distributions of trapped electron (0.19 -3.2 MeV) omnidirectional fluxes observed by OZHORA at 400 km (left) and 800 km (right) during quiet times ($|D_{st}| < 30nT$) in 1984-87. The five contour levels vary logarithmicall from 10^2 to 10^6 $cm^{-2}s^{-1}$ [from Fung *et al.*, 1996].

6. SUMMARY AND CONCLUSIONS

The NASA AP-8MIN model has been found to be consistent with recent trapped proton observations (0.08-2.5 MeV) obtained by the NOAA-10 satellite. Furthermore, only slight variation of the model is seen when it is cast against different IGRF magnetic field models (see Figures 1 and 2).

Good agreement in the low altitude L-shell profiles of trapped electrons has also been found between the diffusive Salammbo model and *in situ* observations by OHZORA at L < 5 (as shown in Figures 3 and 5). The classical diffusive model also performs better than the AE-8 model in terms of predicting the radiation belt structure at low altitudes for L < 3 and E > 0.2 MeV. At L > 5, the discrepancies between the diffusive model and measurements (Figures 8 and 9) are attributable to (1) inaccuracies of AE-8 at low altitude and at L near 7, (2) inaccuracies in D_{LL} at low pitch angles, and (3) uncertainties in the plasmaspheric hiss distribution. Possible improvements of the diffusive model calculations may also include increasing the resolutions in M, J, L, and time so that dynamic effects of the outer radiation belt and geomagnetic activity-dependent transport can be included for the construction of a new generation of trapped radiation models [Fung, 1996].

ACKNOWLEDGMENTS

We thank Drs. T. Kohno (IPCR, Saitama, Japan) and K. Nagata (Tamagawa University, Tokyo, Japan) for providing the OHZORA data to the National Space Science Data Center (NSSDC). Work by Hughes STX was supported through NASA contract NAS5-30960.

REFERENCES

Baker, D. N., J. B. Blake, L. B. Callis, J. R. Cummings, D. Hovestadt, S. Kanekal, B. Klecker, R. A. Mewaldt, and R. D. Zwickl, Relativistic electron acceleration and decay time scales in the inner and outer radiation belts: SAMPEX, *Geophys. Res. Lett.*, **21**, 409-412, 1994.

Beutier T., D. Boscher, M. France, Salammbo: a three-dimensional simulation of the proton radiation belt., *J. Geophys. Res.*, **100**, 17181, 1995.

Beutier, T., and D. Boscher, A three-dimensional analysis of the electron radiation belt by the Salammbo code, *J. Geophys. Res.*, **100**, 14853-14861, 1995.

Boscher, D. M., S. F. Fung, and L. C. Tan, Spatial distributions of the inner radiation belt electrons: a comparison between observations and radial diffusion theory predictions, *Adv. Space Res.*, to be published, 1996.

Fischer, H. M., V. W. Auschrat, and G. Wibberenz, Angular distribution and energy spectra of protons of energy $5 \leq E \leq 50$ MeV at the lower edge of the radiation belt in equatorial latitudes, *J. Geophys. Res.*, **82**, 537, 1977.

Fung, S. F., Recent development in the NASA trapped radiation models, in *Radiation Belts*, edited by J. Lemaire, D. Heynderickx, and D. N. Baker, Geophys. Monogr. 97, American Geophysical Union, Washington, D. C., in press, 1996.

Fung, S. F., L. C. Tan, D. Bilitza, D. Boscher, and J. F. Cooper, An investigation of the spatial variations of the energetic trapped electrons at low altitudes, *Adv. Space Res.*, to be published, 1996.

Gussenhoven, M. S., E. G. Mullen and D. Brautigam, Phillips Laboratory Space Physics Division Radiation Belt Models, in *Radiation Belts*, edited by J. Lemaire, D. Heynderickx, and D. N. Baker, Geophys. Monogr. 97, American Geophysical Union, Washington, D. C., in press, 1996.

Kessel, R. L., R. E. McGuire, R. M. Candey, R. Burley, S. F. Fung, G. Galiardi, T. Kovalick, H. K. Hills, S.-Y. Hsieh, and S. Boardsen, CDAW 10 User Interface Design (Working Version 1.0), 1994a.

Kessel, R. L., R. E. McGuire, H. K. Hills and J. Love, ISTP guidelines for CDF, in the International Solar-Terrestrial Physics (ISTP) Key Parameter Generation Software (KPGS) Standatds and Conventions, ISTP internal document, 1994b.

Kohno, T., K. Munakata, K. Nakada, H. Murakami, A. Nakamoto, N. Hasebe, J. Kikuchi, and T. Doke, Intensity maps of MeV electrons and protons below the radiation belt, Planet. Space Sci., **38**, 483, 1990.

Li, X., I. Roth, M. Temerin, J. R. Wygant, M. K. Hudson, and J. B. Blake, Simulation of the prompt energization and transport of radiationbelt particles during the March 24, 1991 SSC, *Geophys. Res. Lett.*, **20**, 2424-2426, 1993.

Lyons, L. R., and R. M. Thorne, Equilibrium structure of radiation belt electrons, J. Geophys. Res., **78**, 2142, 1973.

Lyons, L. R., R. M. Thorne, and C. F. Kennel, Pitch-angle diffusion of radiation belt electrons within the plasmasphere, J. Geophys. Res., **77**, 3455, 1972.

McCormack, P. D., Radiation Dosage and Shielding for the Space Station, Acta Astronautica, 17(2), 231, 1988.

Nagata, K., T. Kohno, H. Murakami, A. Nakamoto, N. Hasebe, T. Takenaka, J. Kikuchi, and T. Doke, OHZORA high energy particle observations, J. Geomag. Geoelectr., **37**, 329, 1985.

Raben, V. J., D. S. Evans, H. H. Sauer, S. R. Sahm, and M. Huynh, *TIRO/NOAA Satellite Space Environment Monitor Data Archive Documanetation: 1995 Update*, NOAA Technical Memorandum ERL SEL-86, Sapce Environment Laboratory, Boulder CO, 1995.

Roederer, J. G, *Dynamics of Geomagnetically Trapped Radiation*, Springer-Verlag, New York, 1970

Sawyer, D. M., and J. I. Vette, AP-8 trapped proton environment for solar maximum and solar minimum, National Space Science Data Center, NSSDC/WDC-A-R&S 76-06, Greenbelt, MD, 1976.

Schulz, M, *Geomagnetism*, **4**, Academic Press, New York, 87-293, 1991

Schulz, M. and L. J. Lanzerotti, *Particle Diffusion in the Radiation Belts*, Springer-Verlag, New York, 1974.

Seale, R. A., and R. H. Bushnell, *The TIROS-N/NOAA A-J Space Environment Monitor Subsystem*, NOAA Technical Memorandum ERL SEL-75, 1987.

Spjeldvik, W. N. and P. L. Rothwell, The Radiation Belts, in *Handbook of Geophysics and the Space*

Environment, edited by A. S. Jura, Air Force Geophysics Laboratory, pp. 5-1 – 5-55, 1985.

Tan, L. C., S. F. Fung, J. F. Cooper, and D. S. Evans, Global distribution of trapped electrons at low altitudes from OHZORA and the NASA trapped radiation models, *J. Geophys. Res.*, to be submitted, 1996.

Thorne, R. M., E. J. Smith, R. K. Burton, and R. E. Holzer, Plasmaspheric hiss, *J. Geophys. Res.*, **78**, 1581, 1973.

Vette, J. I., *The NASA/National Space Science Data Center Trapped Radiation Environment Model Program (1964-1991)*, NSSDC Publications, 91-29, 1991a.

Vette, J. I., *The AE-8 Trapped Electron Model Environment,* NSSDC/WDC-A-R&S **91-24**, NASA Goddard Space Flight Center, Greenbelt, Maryland, November, 1991b.